The Southeastern Tropical Atlantic SST bias investigated with a coupled atmosphere-ocean single column model at a PIRATA mooring site.

Anna-Lena Deppenmeier* and Rein J. Haarsma† and Chiel van Heerwaarden‡ and Wilco Hazeleger§

Wageningen University, Meteorology and Air Quality, Wageningen, Netherlands

**Corresponding author address:* Anna-Lena Deppenmeier

E-mail: deppenme@ucar.edu

†Royal Dutch Meteorological Institute (KNMI), Research and Development of Weather and Climate Models, De Bilt, Netherlands

‡Wageningen University, Meteorology and Air Quality, Wageningen, Netherlands

§Utrecht University, Faculty of Geosciences, Utrecht, Netherlands

Early Online Release: This preliminary version has been accepted for publication in *Journal of Climate*, may be fully cited, and has been assigned DOI 10.1175/JCLI-D-19-0608.1. The final typeset copyedited article will replace the EOR at the above DOI when it is published.

ABSTRACT

Warm sea surface temperature biases (SST) in the tropical Atlantic form a longstanding problem in coupled general circulation models (CGCMs). Considerable efforts to understand the origins of these biases and alleviate them have been undertaken, but state-of-the-art CGCMs still suffer from biases very similar to those of the generation of models before. In this study, we use a powerful combination of in-situ moored buoy observations and a new coupled ocean-atmosphere single column model (SCM) with identical parameterization as a three dimensional CGCM to investigate the SST bias. We place the SCM at the location of a PIRATA mooring in the southeastern tropical Atlantic, where large SST biases occur in CGCMs. The SCM version of the state-of-the-art coupled GCM EC-Earth performs well for the first five days of the simulation. Then, it develops an SST bias very similar to that of its three dimensional counterpart. Through a series of sensitivity experiments we demonstrate that the SST bias can be reduced by 70 %. We achieve this result by enhancing the turbulent vertical ocean mixing efficiency in the ocean parameterization scheme. The under-representation of vertical mixing in three dimensional CGCMs is a candidate for causing the warm SST bias. We further show that surface shortwave radiation does not cause the SST bias at the location of the PIRATA mooring. Rather, a warm atmospheric near-surface temperature bias and a wet moisture bias contribute to it. Strongly nudging the atmosphere to profiles from reanalysis data reduces the SST bias by 40 %.

Accepted for publication in *Journal of Climate*. DOI 10.1175/JCLI-D-19-0608.1.

1. Introduction

Tropical Atlantic sea surface temperatures (SST) display large variability on inter-annual timescales, and a strong seasonal cycle. State of the art coupled general circulation models (CGCMs) struggle to capture the cooling in the southeastern tropical Atlantic, as a result of which they suffer from large warm SST biases in that region (Richter and Xie 2008; Richter et al. 2012; Wang et al. 2014). These biases hamper efforts to reliably predict societal relevant climate events (Stockdale et al. 2006), such as the West African Monsoon and the Atlantic Niño.

In boreal summer, the southeastern tropical Atlantic cools strongly and rapidly. Simultaneously, a cold tongue forms on the equatorial eastern Atlantic, extending as far as 20^{o}W (Fig. 1a, visible in June, July, and August). In boreal fall, the cold tongue recedes and the cold waters in the southeast warm gradually.

On the southeastern edge of the cold tongue (6^{o}S, 8^{o}E), located in the region of strong annual cooling (Fig. 1b), the Prediction and Research Moored Array in the Tropical Atlantic (PIRATA (Servain et al. 1998; Bourlès et al. 2008)) offers observational data to fill the gap of our knowledge of the ocean and air-sea interaction processes in this region. At the location of this buoy, SST cool by several degrees during boreal summer (Fig. 1b). The cooling in three dimensional CGCMs is much weaker, as indicated at the example of EC-Earth, also in Fig. 1b. The insufficient cooling leads to the large typical positive SST biases in the region. The largest SST biases occur very close to the coast around the Angola Benguela Frontal Zone (Xu et al. 2014a), where biases can be as large as 8°C (Koseki et al. 2018). Harlass et al. (2015) and Milinski et al. (2016) have recently shown the importance of atmospheric resolution for reducing these coastal biases, and Small et al. (2014) stressed the importance of an additional high resolution ocean component. Smaller, but sizeable biases are found at the location of the buoy (Toniazzo and Wool-

Accepted for publication in *Journal of Climate*. DOI 10.1175/JCLI-D-19-0608.1.

nough 2014; Voldoire et al. 2019). During the first five months of the year, the three dimensional model accurately captures the SST in the southeastern tropical Atlantic. With the onset of the strong cooling the bias develops, it is first sizeable in June. This makes June the ideal month to study the bias, as it is the month in which it establishes.

Recently, the seasonal heat budget at this site has been analysed by (Scannell and McPhaden 2018) for the five years in which daily data record is available. The authors find that in boreal summer horizontal advection contributes in a minor role to the heat budget, and that rather reduced shortwave forcing and vertical turbulent entrainment into the upper ocean mixed layer are the main causes for the SST cooling. The latter process occurs at scales too small to be explicitly captured in the ocean component of three dimensional models, and has to be added via parameterization. The specifics of the parameterization determine the strength of the mixing included in the model. The underrepresentation of this vital process is a strong candidate for producing the warm bias (Hazeleger and Haarsma 2005; Exarchou et al. 2017; Planton et al. 2018).

Other origins of the warm bias have been suggested to arise in the atmosphere, for example, from excessive shortwave radiation (Huang et al. 2007; Hu et al. 2008), or insufficient wind forcing (Richter et al. 2012; Voldoire et al. 2014; Koseki et al. 2018), or from an atmospheric moisture bias (Hourdin et al. 2015). A recent multi-model study highlights the role of wind stress forcing in the bias development (Voldoire et al. 2019), but also shows that it cannot explain the entire bias and sometimes even has limited effect (as is the case for EC-Earth, which we use here). Other studies have highlighted the contribution of the ocean model (Xu et al. 2014b), its horizontal and vertical resolution (Seo et al. 2006; Doi et al. 2012; Small et al. 2014), advection (Goubanova et al. 2019) and turbulent processes (Hazeleger and Haarsma 2005; Exarchou et al. 2017; Planton et al. 2018) to the bias formation. The question of the southeastern tropical Atlantic warm bias is not yet resolved and more analysis is clearly necessary to trace its origins.

Accepted for publication in *Journal of Climate*. DOI 10.1175/JCLI-D-19-0608.1.

In this study, we use an ocean-atmosphere coupled single column version of the coupled GCM EC-Earth (Hazeleger et al. 2010) to investigate the bias formation in the southeastern tropical Atlantic, at the location of the 6^{o}S, 8^{o}E PIRATA mooring. With the single column model (SCM) we can investigate processes active on very short time scales. This is impractical, if not impossible, with the three dimensional model. With the coupled SCM, as opposed to the standalone version of the atmosphere and the ocean, we can investigate coupled air-sea processes, and the effect of the model bias in one component on the other component. In this work we first test the impact of the atmosphere on the ocean, and then focus on ocean parameterization.

The short runtime of the SCM allows us to perform a range of sensitivity experiments and explore the parameter space that determines the short timescale processes of our interest. By choosing a location for which in-situ data are available, we are able to closely compare and evaluate the model performance. Additionally, we can employ observed data to force the model.

The paper is structured as follows. We describe the model in Section 2. In Section 3 we describe the data used in this study, and the set up of the SCM experiments. Within Section 4, we evaluate the SCM performance (a), before moving on to atmospheric sensitivity experiments (b) and ocean experiments (c). The results are summarised and discussed in Section 5.

2. Model description

We use a novel coupled ocean-atmosphere SCM Hartung et al. (2018) derived from the three dimensional host model EC-Earth (after Hazeleger et al. (2010, 2012)). Optimal settings for SCM experiments are explored in (Hartung et al. 2018), where the model is initially described. Here, we briefly repeat the description of the model setup.

The SCM consists of the NEMO ocean model version 3.6 (Madec et al. 2011), which includes the sea ice model LIM3 (Vancoppenolle et al. 2008), and the Open Integrated Forecasting System

Accepted for publication in *Journal of Climate*. DOI 10.1175/JCLI-D-19-0608.1.

cycle 40r1 (`https://confluence.ecmwf.int/display/OIFS/About+OpenIFS`) for the atmosphere, with the land surface model H-Tessel (Balsamo et al. 2009). Coupling between the ocean and atmosphere is handled by OASIS3-MCT (Valcke 2013), similar to the way the components couple in three dimensional EC-Earth.

OpenIFS solves the one dimensional primitive equations for momentum (Eqs. 1 and 2), thermodynamics (Eq. 3), and moisture (Eq. 4) for the atmosphere:

$$\frac{\partial u}{\partial t} = -\dot{\eta}\frac{\partial u}{\partial \eta} + F_u + f\,(v - v_g) + P_u + \frac{u_r - u}{\tau_a} \tag{1}$$

$$\frac{\partial v}{\partial t} = -\dot{\eta}\frac{\partial v}{\partial \eta} + F_v - f\,(u - u_g) + P_v + \frac{v_r - v}{\tau_a} \tag{2}$$

$$\frac{\partial T}{\partial t} = -\dot{\eta}\frac{\partial T}{\partial \eta} + F_T + \frac{RT\omega}{c_p p} + P_T + \frac{T_r - T}{\tau_a} \tag{3}$$

$$\frac{\partial q}{\partial t} = -\dot{\eta}\frac{\partial q}{\partial \eta} + F_q + P_q + \frac{q_r - q}{\tau_a} \tag{4}$$

The vertical coordinate η merges orography with pressure coordinates in the free atmosphere. $\dot{\eta}$ is the vertical velocity in this coordinate, and ω the vertical velocity in pressure coordinates. u and v are the horizontal velocity components, with their geostrophic contributions u_g and v_g. f is the Coriolis parameter, R the universal gas constant and c_p the heat capacity (both for moist air). p is pressure. The terms F_i are horizontal advection of momentum, temperature and moisture, and P_i are parameterizations of sub-grid scale processes. The parametrised processes include radiative transfer, convection, and clouds, with its own prognostic equations for cloud liquid and ice, rain and snow water content and cloud cover. These parameterizations have been the subject of intensive research, and are not the focus of this study. Profiles can be nudged to reference states for u_r, v_r, T_r, and q_r with a timescale τ_a.

Accepted for publication in *Journal of Climate*. DOI 10.1175/JCLI-D-19-0608.1.

The surface energy budget is

$$
\begin{aligned}
&(1-\alpha_i)\left(1-f_{R_s,i}\right)R_s + R_T - \varepsilon\sigma T_{sk,i}^4 + SH_i + LH_i \\
&\qquad = Q_T = \Lambda_{sk,i}\left(T_{sk,i}-T_1\right).
\end{aligned}
\tag{5}
$$

The subscript i indicates that the surface grid box is subdivided into tiles, and hence a single gridbox can consist of partly ocean and partly sea ice (or land surface). The shortwave radiation at the surface R_s is absorbed with fraction $f_{Rs,i}$ and reflected with albedo α_i. R_T is downward longwave radiation, ε the surface emissivity, and σ the Stefan-Boltzmann constant. Q_T is the total surface heat flux, and $T_{sk,i}$ and $\Lambda_{sk,i}$ are tiled skin layer temperature and conductivity, respectively. T_1 is the upper ocean (or sea ice) layer temperature. In our case there are ocean tiles only.

The one dimensional ocean model is based on the hydrostatic equation, temperature (T) and salt (S) conservation (Eqs. 8 and 9), the momentum equations (Eqs. 6 and 7), and the equation of state $\rho = \rho\,(T,S,p)$ (polyEOS80-bsq function in Fofonoff and Millard Jr (1983)).

$$\frac{\partial u}{\partial t} = -\frac{\partial}{\partial z}A_{vm}\frac{\partial u}{\partial z} + fv \tag{6}$$

$$\frac{\partial v}{\partial t} = -\frac{\partial}{\partial z}A_{vm}\frac{\partial v}{\partial z} - fu \tag{7}$$

$$\frac{\partial T}{\partial t} = -\frac{\partial}{\partial z}A_{vt}\frac{\partial T}{\partial z} + \frac{1}{\rho_o c_p}\frac{\partial I(F_{sol},z)}{\partial z} + Q_T \tag{8}$$

$$\frac{\partial S}{\partial t} = -\frac{\partial}{\partial z}A_{vt}\frac{\partial S}{\partial z} + E - P \tag{9}$$

f is the Coriolis parameter as above, ρ_o is the ocean reference density 1035 $\frac{kg}{m^3}$, u and v are the horizontal momentum components. The first terms on the right hand side of Equations 6–9 describe the effect of turbulent mixing on the ocean column. A_{vm} and A_{vt} are the vertical turbulent viscosity and diffusivity coefficients, respectively. The coefficients have to be determined via a turbulence closure paramterisation scheme, which is described below. In the one dimensional model, vertical turbulent mixing is the only parametrised process. $I(F_{sol,z})$ is the penetrative part of the surface solar radiation, and $E-P$ is the fresh water flux at the ocean surface due to evaporation

Accepted for publication in *Journal of Climate*. DOI 10.1175/JCLI-D-19-0608.1.

and precipitation. Nudging to reference profiles is, at the moment, not implemented in the model. Scannell and McPhaden (2018) find horizontal advection to play only a very minor role in the heat budget, which justifies the use of the 1D model without applying large scale forcing at this location.

At the coupling interface between the atmosphere and the ocean, the ocean receives wind stress, turbulent, and radiative surface fluxes (split into solar and non-solar), and the fresh water budget from the atmosphere. This impacts the boundary conditions of the ocean according to the following equations, where z is the depth of the column, and τ_u and τ_v are the horizontal wind stress components.

$$A_{vm}\frac{\partial u}{\partial z} = \frac{\tau_u}{\rho_0} \tag{10}$$

$$A_{vm}\frac{\partial v}{\partial z} = \frac{\tau_v}{\rho_0} \tag{11}$$

$$A_{vt}\frac{\partial T}{\partial z} = \frac{Q_t}{\rho_0 c_p} \tag{12}$$

$$A_{vt}\frac{\partial S}{\partial z} = \frac{(E-P)S_0}{\rho_0} \tag{13}$$

The setup of the SCM and the processes relavant to this study are schematically shown in Fig. 2.

a. Turbulent Vertical Mixing in the Ocean

As mentioned above, the sub-grid scale paramterisation in the SCM consists solely of turbulent vertical mixing. It is based on a turbulent kinetic energy (TKE) closure scheme (Blanke and Delecluse 1993; Gaspar et al. 1990; Madec et al. 2011), which solves for the turbulent coefficients A_{vt} and A_{vm} with the prognostic TKE equation:

$$\begin{aligned}\frac{\partial \bar{e}}{\partial t} = \frac{C_{WI}\cdot|\tau|}{\rho_0} + \frac{{w_{LC}}^3}{H_{LC}} + A_{vm}\left[\left(\frac{\partial u}{\partial z}\right)^2 + \left(\frac{\partial v}{\partial z}\right)^2\right] - A_{vt}\cdot N^2 \\ + \frac{\partial}{\partial z}\left[A_{vm}\frac{\partial \bar{e}}{\partial z}\right] - C_{\varepsilon}\frac{\bar{e}^{\frac{3}{2}}}{l_{diss}} + C_{WF}\cdot\bar{e}\cdot exp^{-z}\end{aligned} \tag{14}$$

Accepted for publication in *Journal of Climate*. DOI 10.1175/JCLI-D-19-0608.1.

The change of available TKE $\bar{e}$ in time is the sum of the following contributions to the TKE budget, in the order of appearance on the right hand side: production by wind input at the surface, Langmuir cell contributions, production by shear, destruction by stratification, vertical diffusion, Kolmogorov dissipation, and internal and surface wave breaking. In Equation 14, C_{WI} is a parameter for the wind input, $|\tau|$ is the wind stress, ω_{LC} is the Langmuir circulation velocity, and H_{LC} the depth of the Langmuir cell. The Langmuir circulation strength is calculated according to

$$w_{LC} = C_{LC} \cdot u_s \cdot sin(\frac{\pi z}{H_{LC}}), \tag{15}$$

with $u_s = 0.377 \cdot \sqrt{|\tau|}$, H_{LC} is dependent on the column stability given by N^2, and C_{LC} is a coefficient influencing the circulation strength.

Furthermore, N^2 is the Brunt-Väisälä frequency, C_ε and l_{diss} are the dissipation coefficient and length scale. The latter is calculated according to

$$l_{diss} = \sqrt{\frac{2\bar{e}}{N^2}}, \tag{16}$$

and is furthermore bound by phyical considerations (e.g., the length close to the surface cannot be larger than the distance to the surface). C_{WF} is the wave breaking coefficient indicating the fraction of energy that penetrates below the mixed layer.

The turbulent coefficients A_{vm} and A_{vt}, vertical eddy viscosity and diffusivity, are calculated according to Eqs. 17 and 18:

$$A_{vm} = C_{diff} \cdot l_{mix} \cdot \sqrt{\bar{e}} \tag{17}$$

$$A_{vt} = A_{vm}/P_{rt} \tag{18}$$

Here, C_{diff} is a coefficient for which the numerical value has to be derived from observations, it is related to the vertical eddy mixing efficiency (Gaspar et al. 1990). l_{mix} is the mixing length across which the turbulence can act, equal to l_{diss}. The Prandtl Number P_{rt} in Eq. 18 is dependent on the

Accepted for publication in *Journal of Climate*. DOI 10.1175/JCLI-D-19-0608.1.

Richardson Number $Ri = \frac{N^2}{\left(\frac{\partial U}{\partial z}\right)^2}$, but in fact is equal to 1 in all cases considered. Hence, A_{vm} and A_{vt} have the same value.

Of the coefficients denoted by C_i, some are more certain than others. C_ε, for example, is generally agreed to take on the value 0.7 (Gaspar et al. 1990). Similarly, C_{WI} (wind input coefficient) and C_{WF} (wave fraction penetration below the mixed layer) are chosen to represent the average impact of medium aged waves. The Langmuir Coefficient, on the other hand, is set to 0.15 as a default, but can assume values up to 0.45 (Axell 2002). C_{diff} can be estimated according to:

$$C_{diff} = \frac{1}{2} \cdot \gamma \cdot P_{dl} * C_\varepsilon, \tag{19}$$

where $C_\varepsilon = 0.7$ and $P_{dl} = 1$. For the ocean vertical mixing efficieny γ, observational estimates exist. From these measurements it results that C_{diff} can assume values between 0.035 and 0.28 (Gaspar et al. 1990). Osborn (1980) estimates $C_{diff} = 0.07$, Oakey (1982) finds C_{diff} between 0.04 and 0.13, Moum et al. (1989) suggest a value between $C_{diff} = 0.04$ and 0.17, Lilly et al. (1974) find $\gamma = 0.33$, and therefore $C_{diff} = 0.1$, and Weinstock (1978) suggests $C_{diff} = 0.28$. The default value in NEMO, C_{diff} = 0.1, is on the lower end of the possible values for C_{diff}. Considering the large observational uncertainty, we propose experiments investigating the climate system sensitivity this parameter.

3. Experimental Setup

The SST bias in CGCMs typically peaks in boreal summer, coinciding with the period of rapid observed cooling. We first examine whether the SCM displays similar behaviour, focusing on June, when the observed cooling is strongest and the bias begins to develop. We perform an ensemble of five simulations for the years in which there are high temporal resolution buoy observations available (2014-2018).

Accepted for publication in *Journal of Climate*. DOI 10.1175/JCLI-D-19-0608.1.

To account for large scale circulation impacts, the SCM is forced with horizontal wind, temperature and moisture advection. This forcing is extracted from 3-hourly ERA-Interim data (Dee et al. 2011) from the grid point closest to the buoy. The grid point is approximately 50 km away (5.96^{o}S, 8.44^{o}E). We assume that the large scale circulation in the region is spatially homogeneous enough to justify using the data of this gridpoint for forcing the experiments, rather than averaging over a box around the buoy. Additionally, the vertical profiles of wind, temperature and moisture above 3 km are nudged to ERA-Interim profiles with a relaxation timescale $\tau_a = 6$ hours. This ensures realistic evolution of the atmosphere, while leaving sufficient freedom in the marine boundary layer. ERA-Interim data is also used to validate the atmosphere column simulation. Additionally, we use high temporal resolution shortwave radiation data from the buoy.

For the ocean initialisation we use daily vertical temperature and salinity profiles from the PIRATA buoy (Servain et al. 1998; Rouault et al. 2009). Temperature data is available down to 500 m, and salinity down to 120 m. Below these depths, we extend the profiles with monthly mean profiles from the ECMWF ocean reanalysis system ORAS4 (Balmaseda et al. 2013). These are adjusted to match the bottom temperature and salinity of the buoy data. From there the ocean evolves freely throughout the simulation, without nudging to reference profiles. Chlorophyll data from Sea-viewing Wide Field-of-view Sensor Ocean Color Data from the NASA Goddard Space Flight Center is used to take into account heating by solar penetration (Center and Laboratory 2014).

a. Sensitivity Experiments

The sensitivity experiments performed for this study are listed in Table 1. Only settings that deviate from the control experiment are specified in the table.

Accepted for publication in *Journal of Climate*. DOI 10.1175/JCLI-D-19-0608.1.

First, we test the impact of atmospheric biases on SSTs. We perform a simulation in which we replace the shortwave radiation the ocean receives with observed shortwave radiation from buoy data (experiment ”Shortwave”).

Furthermore, to test the contribution of other surface fluxes we perform an experiment in which we nudge the horizontal wind components, as well as the temperature and moisture profiles from ERA-Interim down to the surface with a relaxation timescale that is equal to the model timestep (15 min, ”UVTQ ERA”). In two separate experiments we nudge only the horizontal wind components to ERA-Interim profiles, and T and Q to control profiles, and vice versa (experiments “U,V ERA” and “T,Q ERA”).

Secondly, we perform sensitivity experiments in which we test the intrinsic ocean contribution to the SST bias. In the absence of advection, we focus on the parameterization of vertical turbulent mixing. Two coefficients in this scheme lend themselves for sensitivity experiments: C_{LC} and C_{diff}. Both parameters are highly uncertain, due to differing measurement results by which they are constrained. As mentioned above, C_{LC} is set to 0.15 as a default, but can physically be as large as 0.45 (Axell 2002). In ”C_{LC} sweep” we perform a suite of sensitivity experiments in which we vary this parameter.

In the sensitivity experiment suite ”C_{diff} sweep” we test the impact of C_{diff} by performing a sweep of SCM integrations in which we vary its value in the physical plausible possible range between 0.035 and 0.28 (see Section a).

Lastly, we test the influence of ocean stratification on the calculation of the vertical turbulent coefficients. Stratification enters the computation of the turbulent coefficients via the Brunt-Väisälä Frequency N^2, the frequency at which a displaced mass element oscillates around its location in a static case. N^2 is used to calculate the mixing length l_{mix}, the distance across which the turbulent

Accepted for publication in *Journal of Climate*. DOI 10.1175/JCLI-D-19-0608.1.

mixing can act (equal to the dissipation length scale l_{diss}, Eq. 16).

$$l_{mix} = l_{diss} = \sqrt{\frac{2\bar{e}}{N}}. \tag{20}$$

Via the mixing length, N enters into the calculation of the vertical eddy coefficients (Eq. 17). In the sensitivity experiment "$N^2{}_{PIR}$", we test the impact of (erroneous) model stratification on the SST bias. Instead of allowing the model to calculate N^2 from its own active tracer profiles, we replace them with high temporal resolution profiles from observations. The replacement happens at the point where N^2 is calculated exclusively, and is not equivalent to ocean nudging.

4. Results

a. Temperature bias in the Single Column Model

During the first four days of the simulation, the SCM ensemble follows the observed cooling very well (Fig. 3a). In that time, SST cool by almost a degree in both the observations and the model. However, the daily cycle is considerably stronger in the model than in the observations. Both the daily maximum and minimum SST are over-/underestimated by the model.

After the initial phase, observed SST continue to decrease strongly, in total by almost three degrees at the end of the month. The model cools by less than two degrees. In a gradual build-up, the SST bias grows to 1.1 ^{o}C at the end of the simulation. This bias is smaller than that of most state-of-the-art coupled GCMs, but it is only slightly smaller than the bias in the three dimensional version of EC-Earth (Exarchou et al. 2017; Voldoire et al. 2019, and Fig. 1b). The SST bias in this region in initialised EC-Earth simulations grows to approximately one degree during June (Deppenmeier et al. under review at Climate Dynamics).

For the sensitivity experiments in this paper, we choose a year that represents the ensemble average well. In 2014, model SSTs follow observed SSTs closely during the first five days (Fig. 3b).

Accepted for publication in *Journal of Climate*. DOI 10.1175/JCLI-D-19-0608.1.

Daily maximum temperatures are overestimated, much like in the ensemble average. From day six onwards, the SCM cannot reproduce the observed cooling. A warm SST bias builds up gradually, and reaches two degrees at the end of the month.

In the control simulation the SCM displays a root mean square error (RMSE) in atmospheric temperature of 0.81^{o}C and moisture excess of $9.2{\cdot}10^{-4}$ kg/kg in the lowest kilometer of the atmosphere (see comparison SCM and ERA-Interim, Fig. 4, upper panels). The qualitative evolution of both moisture and temperature is well captured by the model. The air cools and dries throughout June. However, the SCM the column is too warm and too moist. The wet bias is already present at the very beginning of the simulation, when SST are still very close to the ones observed. This indicates that it arises in the atmosphere. It is indeed also present in an atmosphere only (AMIP-type) simulation (not shown). The 10m temperature warm bias grows with time, but the wet bias is largest in the beginning and remains relatively stable thereafter. Near-surface temperatures in an AMIP type simulation are cooler than in the coupled simulation, especially after 5-10 days of runtime (not shown).

Below the ocean surface, temperatures in the first 10 meters decrease steadily throughout the month in the buoy measurements (Fig. 4, bottom panel left hand side). At depth between 10 and 30 m, the measurments show very short time scale variability, leading to rapid and short-lived deepening and shallowing of the thermocline. Near-surface ocean temperatures in the SCM also decrease, but less so than in observations. In the model, the thermocline deepens monotonically and diffuses throughout the month (Fig. 4, bottom panel right hand side). This trend is not visible in the observational data. Similar to what we have observed for the daily cycle of SST, upper ocean temperature in the SCM displays a stronger diurnal cycle than the buoy data. In the model, a shallow warm near-surface layer of up to 10 m depth develops every day.

Accepted for publication in *Journal of Climate*. DOI 10.1175/JCLI-D-19-0608.1.

The control simulation surface fluxes show of a relatively constant shortwave radiation input, and similarly constant radiative and turbulent cooling (Fig 5). In total, the SCM surface fluxes warm the ocean. The observed cooling therefore must be a result of cooling from below, which in the absence of advection must be caused by vertical turbulent entrainment of cold water into the warm surface layer.

To summarise, the SCM performs very well during the first days of the simulation. Thereafter, it rapidly develops a SST bias very similar to that of its three dimensional counterpart. Atmospheric moisture is overestimated from the beginning of the simulation, and surface atmospheric temperatures increase simultaneously with the SST bias.

In the following, we investigate different reasons for the model biases and possibilities to alleviate them. First, we focus on impacts arising in the atmosphere in section b, and then on the ocean model itself in section c.

b. Surface forcing

A possible explanation for the warm SST bias could be excess shortwave radiation, which artificially heats the sea surface. This has been suggested for the eastern boundary region in the Pacific (Ma et al. 1996), and might be true also for the Atlantic (Huang et al. 2007; Hu et al. 2011; Zuidema et al. 2016). We investigate this possibility with two approaches. First, we compare the surface shortwave radiation from the SCM to the buoy measurements, to establish whether a positive shortwave radiation bias is present.

At first glance, the surface shortwave radiation time series of the SCM seems to suffer from a shortage of radiation rather than a surplus on most days in the simulation (Fig. 6). However, the two data sets cannot readily be compared, because of their differing time resolution. Model data is available on 15 minute intervals, while buoy data is provided at 2 minute intervals. To eliminate

Accepted for publication in *Journal of Climate*. DOI 10.1175/JCLI-D-19-0608.1.

the apparent differences arising from differences in temporal resolution, and therefore differences in the representation of intermittency, we compute daily integrals of shortwave radiation (Fig. 7). The integrated daily amount of surface short wave radiation in the SCM is very similar to the one observed. The difference between the total energy input during the length of the simulation depends only slightly on whether the original 2-minute data from PIRATA is used or whether PIRATA data is interpolated to the 15 minute resolution of the SCM. In the latter case, energy input between the model and the observations only differs by 0.05 %. In the former case the energy difference amounts to 0.5 % excess in the SCM as compared to PIRATA, 2382 kJ over the entire month. This difference is due to the high intermittency of observed surface radiation, which cannot be matched by the SCM output frequency. However, the excess shortwave radiation cannot account for the SST bias. An estimate of the SST tendency term due to heating $\frac{\partial T}{\partial t} = \frac{Q}{h \cdot \rho_w \cdot c_p}$, with an assumed sea water density ρ_w of 1020 kg/m^3 and a specific heat capacity c_p of 4000 J/kg/K and a very shallow mixed layer depth h of 20 m shows that the order of magnitude of heating due to this excess is 0.03^{o}C. The surface solar radiation bias, hence, cannot explain the warm SST bias, which is larger by almost two orders of magnitude. This conclusion is consistent with those of other studies using EC-Earth (Exarchou et al. 2017; Voldoire et al. 2019; Deppenmeier et al. under review at Climate Dynamics).

1) Atmospheric Sensitivity Experiments

Even though the difference in surface shortwave radiation is small, feedbacks involving in it could still influence the SST bias. To test this hypothesis, we perform a coupled simulation in which the ocean receives observed shortwave radiation, instead of the one calculated by the atmospheric component (Experiment “Shortwave”). Consistent with the conclusion from the shortwave radiation analysis, the SST bias in this simulation does not reduce. The SST evolution is hardly

Accepted for publication in *Journal of Climate*. DOI 10.1175/JCLI-D-19-0608.1.

influenced during the time of the simulation (Fig. 8, green line). This solidifies the notion that surface shortwave radiation is not the main origin of the warm SST bias in the southeastern part of the cold tongue.

In Section a, we have seen that the near surface atmosphere in the SCM is warm and wet biased. Both these biases could be a cause or consequence of the warm SST bias. To determine the impact of atmospheric biases on the SST bias, we investigate sensitivity experiments in which the atmosphere is unbiased (with respect to ERA-interim). In this experiment, “Atm ERA”, the SST bias reduces from 1.25 ^{o}C to 0.69 ^{o}C. The observed cooling now matches for approximately 10 days of the simulation (Fig. 8, red line). After that, the steep observed cooling can, again, not be reproduced by the model.

The reduction of SST bias is notable, however, and we investigate the cause further. A possible reason for the warm SST bias originating in the atmosphere is reduced forcing of the ocean due to underestimated winds. This theory has recently been supported by Xu et al. (2014b) and Voldoire et al. (2019). We test the influence of wind biases on the SST bias in experiment “U,V ERA”. The wind forcing hardly impacts the simulation (Fig. 8, purple line). The SST RMSE decreases only by 0.05 ^{o}C. Voldoire et al. (2019) show EC-Earth to be the least sensitive CGCM to the wind stress replacement. This is due to the small wind stress bias in the model compared to ERA-Interim. In the SCM, the wind stress bias is also small. As a consequence, wind stress nudging mostly changes the direction of the wind, but does not enhance its amplitude (not shown). Because the wind bias is small to begin with, this experiment does not much impact the surface flux budget (Fig. 9, panel b), and hence has a very small impact on the RSME SST.

The atmosphere furthermore exerts influence on the ocean surface via surface level temperature and moisture, which impact the surface flux budget. It has recently been suggested that atmospheric moisture is a major cause for the warm SST bias (Hourdin et al. 2015). In the experiment

Accepted for publication in *Journal of Climate*. DOI 10.1175/JCLI-D-19-0608.1.

"T,Q ERA" we remove the model bias of temperature and moisture with respect to ERA-Interim. This experiment is able to almost reproduce the cooling of "Atm ERA". The SST RMSE in this simulation is reduced to 0.69 ^{o}C.

In both experiments in which moisture and temperature are adjusted an increase in turbulent surface fluxes drive the SST cooling by reducing the total surface flux going into the ocean (Fig. 9). The turbulent fluxes cool considerably more when atmospheric temperature and moisture are improved. The total surface flux in the sensitivity experiments with the latter variables from ERA-Interim even changes signal, and now cools the ocean rather than warming it, as in the control.

We have demonstrated the impact of the (near surface) atmosphere conditions as well as shortwave radiation on the SCM SST bias. While shortwave radiation is modeled accurately at the location of the buoy, the warm and moist near surface air bias contribute to the warm SST bias. In bias-reduced atmosphere simulations it is possible to reduce the SST RMSE from 1.25 ^{o}C to 0.69 ^{o}C. This is a considerable reduction, but a sizeable SST bias remains, even if the atmosphere is unbiased. The origin of the remaining bias lies in the ocean interior. Hence, in the following section, we will turn our attention to the ocean.

c. Ocean model

Entrainment of cold water by turbulent vertical mixing plays a large role in the tropical upper ocean heat budget (Foltz et al. 2003; Moum et al. 2013; Hummels et al. 2014; Scannell and McPhaden 2018). If this process is underrepresented, due to, for example, inadequate parameterization, it can lead to warm SST biases. Too little cold water could be entrained into the shallow mixed layer from below, leading too insufficient cooling. In this section we examine influences on vertical turbulent mixing in the upper ocean and their effect on the SST.

Accepted for publication in *Journal of Climate*. DOI 10.1175/JCLI-D-19-0608.1.

The TKE scheme, as described in Section a, adds the contributions to the available TKE, and then infers the turbulent mixing coefficients, which determine mixing in the ocean column. The first source term of TKE is the Langmuir Cell parameterization.

1) Langmuir circulation

Langmuir circulation is dependent on wind input at the surface, and the stability of the ocean column. Langmuir circulation can be an important contribution to entrainment by cool water at the bottom of the mixed layer (Skyllingstad and Denbo 1995). They appear generally above wind speeds of 3 m/s (Talley 2011), which is frequently crossed in our simulations (not shown). The strength of the parametrised circulation is dependent on the coefficient C_{LC}, which has been set to 0.15 by Axell (2002). Its value can be increased, but the recommendation is to keep it below 0.54. Here, we test the whole parameter space between the two values.

Overall, there is a slight decrease in SST RMSE with increasing Langmuir coefficient (Fig. 10, green markers). It is notable, however, that the RMSEs between values of $C_{LC} = 0.15$ and 0.45 are noisy, rather than showing a clear tendency. SST RMSE only decreases more consistently at values larger than 0.45. From the shape of the curve no clear recommendation can be made for the value of C_{LC}, though higher values might be preferred, rather than the very low default value.

2) Vertical mixing efficiency

Next, we test the response to increasing the vertical mixing efficiency in the TKE scheme. The vertical mixing coefficients A_{vt} and A_{vm} depend on C_{diff} that represents the ocean mixing efficiency (Equations 17, 18, and 19). This factor is loosely constrained by measurements, but can assume values between 0.035 and 0.28. Here, we test the parameter space in the same manner as in Section 1.

Accepted for publication in *Journal of Climate*. DOI 10.1175/JCLI-D-19-0608.1.

The SST RMSE is very sensitive to the value of C_{diff} (Fig. 10, blue markers). At the default value $C_{diff} = 0.1$, the RMS SST bias has a value of 1.25 ^{o}C. At lower values, i.e., at less efficient mixing, the bias is even larger (up to 1.87^{o}C at lowest $C_{diff} = 0.035$), growing with decreasing C_{diff}. SST RMSE values decrease rapidly with increasing C_{diff}. The minimum bias is reached at $C_{diff} = 0.23$, the bias then amounts to only 0.32^{o}C. This is a reduction of 74% of the default bias. Between values of 0.2 and 0.25 for C_{diff}, the bias is relatively stable and very low. When C_{iff} is increased further, the SST RMSE increases again. This is due to the model sea surface then becoming too cold, leading to a cold bias with respect to observations.

At the optimal value for C_{diff}, model SST follow observations well (Fig. 11, purple line). Enhancing turbulent vertical mixing in the ocean column within the physically plausible range can reduce the SST bias to approximately a quarter of its original amplitude. The parameter change in C_{diff} enhances the turbulent heat flux (THF) across the mixed layer from 10.3 W/m^2 to 21.5 W/m^2 (estimated from $\frac{\partial T}{\partial t} = Q_{net} + \frac{THF}{\rho \cdot c_p \cdot h}$, with $\rho = 1024$ kg/m^3, $c_p = 4000$ J/kg/K, and the mean diagnostic mixed layer depth $h = 25$). This is in good agreement with values reported in the literature by Foltz et al. (2018) and Scannell and McPhaden (2018).

In the ocean column, the warm top layer formation is reduced with the optimal C_{diff} as compared to the control (Fig. 12, bottom row), but not entirely removed. The diurnal cycle remains too strong compared to observations (as is also evident from SST (Fig. 11)). Short timescale subsurface temperature variability as observed in PIRATA data (Fig. 4) is not present in the model, despite the increased vertical mixing activity.

Consistent with the cooler SST, near surface atmospheric temperatures are also decreased. However, higher up the atmosphere strongly warms as compared to the control (Fig. 12, centre row). The atmosphere was warmer than ERA-Interim to begin with (Fig. 4), hence, this is a degradation of model performance. The overestimation of near surface moisture is increased near the surface,

Accepted for publication in *Journal of Climate*. DOI 10.1175/JCLI-D-19-0608.1.

and aloft a dry region forms that is not observed in ERA-Interim. These atmospheric changes consistently occur in an AMIP type simulation forced with observed SST (not shown). They are hence intrinsic to the atmospheric component of the coupled model, which is not the focus of the current study. Further investigation of this behaviour might be the focus of an atmospheric study.

Surface fluxes along the C_{diff} sweep decrease (Fig. 13). The higher C_{diff}, the cooler the sea surface, and, as a consequence, both the turbulent fluxes and the longwave radiation flux decrease. Shortwave radiation also decreases, though it is more complicated to place this decrease. Cooler surface temperatures might lead to more stratocumulus cloud cover due to increased boundary layer stability, but the response of clouds to the SST is very noisy. The dominant cloud type in the simulations are shallow convection cumulus, which react strongly to perturbations of SST in AMIP type runs due to their chaotic nature (not shown). Considering that shortwave radiation is not overestimated in the control (Fig. 7), the reduced shortwave radiation with increased C_{diff} is not a model improvement. However, it positively influences the SST bias.

3) VERTICAL MIXING EFFICIENCY IN CHANGED SETTING

We have demonstrated the beneficial effect of increasing the vertical ocean mixing on reducing RMSE SST. Setting C_{diff} to a value twice as large as the default value, but still within the plausible physical range, results in a realistic simulation of SST. We have also demonstrated beneficial impact of correctly modelled near surface temperature and moisture in the atmosphere. We wonder whether already improved simulations, as “Atm ERA”, are less sensitive to the value of C_{diff}. Therefore, we perform another set of parameter sweeps along the values of C_{diff} for the nudged atmosphere experiment, and additionally for the shortwave forcing experiment.

Fig. 14 shows SST RMSE depending on the value of C_{diff}. The RMSEs have been fitted with a cubic function, stars mark minimum values on the curve. All three sweeps reach a minimum in the

Accepted for publication in *Journal of Climate*. DOI 10.1175/JCLI-D-19-0608.1.

C_{diff} range between 0.2 and 0.25, and the RMSE at their respective ideal C_{diff} are very similar. The lowest RMSE value is obtained when the atmosphere is nudged to the surface (Fig. 14, red). This suite is also least dependent on the value of C_{diff}, as is indicated by the relatively flat curve. Since the sea surface is already beneficially influenced by cooler near surface temperatures in the atmosphere, the SST bias does not reach values as high as in the control.

All three curves, whether it is the coupled simulation, the atmosphere nudged to the reanalysis state, or the shortwave radiation used from observations, reach their minimum around the same value of C_{diff}, between 0.20 and 0.25 (Fig. 14). The SST biases obtained at these C_{diff} values are very small; meaning that the summertime SST cooling is well represented. This highlights the dominant effect of the vertical turbulent mixing on the ocean cooling. When there is enough vertical mixing, other factors, such as an improved atmosphere, does not much improve the simulation anymore. This result is hence a very strong indication of the importance of vertical turublent mixing, and implies that the value for C_{diff} should be increased in three dimensional simulation. Although the mean bias reduces, the intermittency of the ocean is not captured.

4) Stratification

We have established in Section a that modelled SST as well as the upper 10m of the ocean column display a stronger daily cycle than observed (Figures 4 and 8). This warm top layer artifically stabilises the ocean column. Ocean stability enters the TKE scheme in the form of the Brunt-Väisälä frequency N^2 with a negative sign (Eq. 14). Increased stratification reduces the TKE available to create vertical ocean mixing. Furthermore, the stability enters into the calculation of the mixing length l_{mix} (Eq. 16, and $l_{mix} = l_{diss}$). When $\bar{e}$ decreases due to large N^2, l_{mix} decreases. Additionally, $l_{mix} \propto \frac{1}{N}$, the mixing length decreases even more. l_{mix} enters into the calculation of

Accepted for publication in *Journal of Climate*. DOI 10.1175/JCLI-D-19-0608.1.

the turbulent eddy coefficients via Eqs. 17 and 18. All of these effects cause vertical ocean mixing to decrease with increasing stratification.

Here, we test the effect of stratification on the ocean vertical mixing and on the SST bias. We replace model temperature and salinity with those from high temporal resolution PIRATA observations, which are less stratified. As a result, turbulent vertical mixing is increased (not shown). The enhanced mixing leads to a considerable reduction of the SST RMSE from 1.25 ^{o}C in the control to 0.89 ^{o}C in ${N^2}_{PIR}$. The SST bias is decreased by almost a third. This highlights the impact stratification asserts on ocean vertical mixing. In the SCM, a positive feedback loop involving stratification and vertical mixing likely grows the SST bias. Vertical mixing is insufficiently strong in the beginning, which leads to increased stratification. The ocean stability in turn reduces the TKE, which further decreases vertical mixing.

In the sensitivity experiment, A_{vt} is less intermittent in the upper 5 m than in the control simulation (not shown). The continuously active mixing also occasionally penetrates the upper 10 m of the column, and towards the end of the simulation (day 25) displays very short term, but strong bursts in the upper 20 m. The effect of the enhanced mixing activity on SST is large (Fig. 11, green line). Especially after day 25, when ”deeper” mixing bursts first occur, the sea surface cools considerably more than in the control simulation.

It should be noted that the temperature and salinity fields used in this experiment contain high frequency variability, for example from internal waves. The TKE parameterization includes a term for turbulence production by internal waves (see last term of Equation 14). This could lead to double counting of this specific term on the one hand, and on the other hand some high frequency variability from internal waves might be present in the 3D model that is absent in the SCM.

Accepted for publication in *Journal of Climate*. DOI 10.1175/JCLI-D-19-0608.1.

5. Discussion and Summary

In this study, we use a coupled ocean atmosphere SCM to investigate the warm SST bias in the tropical Atlantic Ocean. Such a bias establishes rapidly in three dimensional coupled global circulation models throughout boreal summer. The warm bias is typically large in the southeast tropical Atlantic and occurs in most CGCMs.

We place the SCM at a PIRATA mooring location in the southeastern tropical Atlantic. This enables us to compare the model simulation to in-situ point observations. For the average of the five years in which high temporal resolution buoy data are available, the SCM version of EC-Earth performs well in the first five days of the simulation. It then produces a SST bias very similar to that in the three dimensional version of the model, the RMSE of the bias is 1.25^{o}C. This makes the SCM a useful tool to investigate the origin of the bias and test possible ways to alleviate it.

For the case of 2014 we eliminate solar surface radiation as the main cause of the warm SST bias. This is in line with other studies (Exarchou et al. 2017; Voldoire et al. 2019; Deppenmeier et al. under review at Climate Dynamics). Forcing the ocean with observed surface shortwave radiation does not improve simulation of the SST. Note that the location in this study coincides with the trade cumulus region. Further southeast, radiation may contribute to, or even be a main cause of model biases. Near surface temperature and moisture in the atmosphere, however, assert a considerable influence on simulated SSTs (producing an RMSE of 0.70^{o}C, a reduction of 44 %). Nudging winds to ERA-Interim profiles, on the other hand, hardly affects the SST. This is to be expected for EC-Earth, which has a relatively small wind bias (Voldoire et al. 2014).

While correcting the atmosphere improves the SST simulation, a sizable bias remains. We show that the bias can be reduced to a quarter of its original size by making physical changes in the ocean model alone. We increase the factor with which TKE is transformed to turbulence within its

Accepted for publication in *Journal of Climate*. DOI 10.1175/JCLI-D-19-0608.1.

physical range by setting the vertical mixing efficiency coefficient C_{diff} from its default value 0.1 to its optimal value 0.23. This reduces the SST bias to 0.34^{o}C, the largest reduction we are able to achieve with any sensitivity experiment. Using the optimal value for C_{diff} also improves the vertical ocean profile. A very stable and warm upper bias, visible in the control simulation, is reduced. However, the intermittency in observations is not captured, even in the experiments with highest mixing efficiency parameters. The large improvement of the ocean simulation with increased vertical mixing hints to vertical mixing being an underrepresented process in the SCM. Similarly, it is likely underestimated in the CGCMs, which use the same vertical mixing parameterization. It is, however, possible that part of the insufficient mixing in the SCM stems from neglecting remote forcing and equatorial/coastal wave propagation. Furthermore, mixing induced by shear variability deeper than the wind driven shear might be underestimated in the current setup of the SCM in comparison the 3D model. Therefore, the ideal value in the SCM is not necessarily the idea value for a CGCM. We recommend research aimed at improving vertical mixing parameterizations for other locations than the one explored here, as well as the impact of horizontal currents.

We test the influence of the Langmuir circulation coefficient. The model sensitivity to this parameter is much smaller than that to C_{diff}, and there is no clear optimal value for C_{LC}.

Furthermore, calculating vertical eddy coefficients with the correctly stratified profiles reduces the SST bias to 0.89^{o}C. Upper ocean mixing is increased with the correct profiles, which reduces the SST bias. The artifical stable stratification in the control simulation leads to decreased mixing, which in turn leads to more stable stratification. This is a positive feedback that worsens the bias. Most likely, initial ocean vertical mixing is too low in the model, which then leads to the artificially stable column. This could hence be alleviated with an increase in the mixing efficiency.

In further experiments, we have also tested the maximum solar penetration depth, which has recently been suggested to assert large influence on SST (Exarchou et al. 2017). In this study,

Accepted for publication in *Journal of Climate*. DOI 10.1175/JCLI-D-19-0608.1.

however, we find no reduction of the bias by increasing the depth from 23 m to either 30 m or 50 m.

In this study, we demonstrate that both the atmosphere and the ocean contribute to the warm SST bias in the southeastern tropical Atlantic. We show that the bias can be considerably reduced by enhancing the vertical ocean mixing efficiency within its physically plausible range. The climate sensitivity to the ocean vertical mixing parameterization in the fully coupled global model EC-Earth is tested in a separate study (Deppenmeier et al. under review), where impacts on the atmospheric circulation and projected climate change are shown. More observations to better constrain the parameter C_{diff} are desirable, so that it can be confirmed whether the larger value is indeed more appropriate for modeling ocean vertical mixing.

Acknowledgments. This study was supported by the EU FP7/2007–2013 PREFACE Project under Grant agreement 603521. We acknowledge the GTMBA Project Office of NOAA/PMEL for the freely available PIRATA mooring data used as model forcing and for comparison. We acknowledge Kerstin Hartung for valuable collaboration and help with identifying optimal settings for the SCM.

References

Axell, L. B., 2002: Wind-driven internal waves and langmuir circulations in a numerical ocean model of the southern baltic sea. *Journal of Geophysical Research: Oceans*, **107 (C11)**.

Balmaseda, M. A., K. Mogensen, and A. T. Weaver, 2013: Evaluation of the ecmwf ocean reanalysis system oras4. *Quarterly Journal of the Royal Meteorological Society*, **139 (674)**, 1132–1161.

Balsamo, G., A. Beljaars, K. Scipal, P. Viterbo, B. van den Hurk, M. Hirschi, and A. K. Betts, 2009: A revised hydrology for the ecmwf model: Verification from field site to terrestrial water

Accepted for publication in *Journal of Climate*. DOI 10.1175/JCLI-D-19-0608.1.

storage and impact in the integrated forecast system. *Journal of hydrometeorology*, **10 (3)**, 623–643.

Blanke, B., and P. Delecluse, 1993: Variability of the tropical atlantic ocean simulated by a general circulation model with two different mixed-layer physics. *Journal of Physical Oceanography*, **23 (7)**, 1363–1388.

Bourlès, B., and Coauthors, 2008: The pirata program. *Bulletin of the American Meteorological Society*, **89 (8)**, 1111–1126, doi:10.1175/2008BAMS2462.1, URL https://doi.org/10.1175/2008BAMS2462.1, https://doi.org/10.1175/2008BAMS2462.1.

Center, N. G. S. F., and O. E. Laboratory, 2014: Sea-viewing wide field-of-view sensor (seawifs) ocean color data. *NASA OB.DAA*.

Dee, D., and Coauthors, 2011: The era-interim reanalysis: Configuration and performance of the data assimilation system. *Quarterly Journal of the royal meteorological society*, **137 (656)**, 553–597.

Deppenmeier, A.-L., R. J. Haarsma, P. LeSager, and W. Hazeleger, under review: The effect of vertical ocean mixing on the tropical atlantic in a coupled global climate model. *Climate Dynamics*.

Deppenmeier, A.-L., R. J. Haarsma, P. LeSager, and W. Hazeleger, under review at Climate Dynamics: The effect of vertical ocean mixing efficiency on the tropical atlantic in a coupled global climate model.

Doi, T., G. A. Vecchi, A. J. Rosati, and T. L. Delworth, 2012: Biases in the atlantic itcz in seasonal–interannual variations for a coarse-and a high-resolution coupled climate model. *Journal of Climate*, **25 (16)**, 5494–5511.

Accepted for publication in *Journal of Climate*. DOI 10.1175/JCLI-D-19-0608.1.

Exarchou, E., C. Prodhomme, L. Brodeau, V. Guemas, and F. Doblas-Reyes, 2017: Origin of the warm eastern tropical atlantic sst bias in a climate model. *Climate Dynamics*, 1–22.

Fofonoff, N. P., and R. Millard Jr, 1983: Algorithms for the computation of fundamental properties of seawater.

Foltz, G. R., S. A. Grodsky, J. A. Carton, and M. J. McPhaden, 2003: Seasonal mixed layer heat budget of the tropical atlantic ocean. *Journal of Geophysical Research: Oceans (1978–2012)*, **108 (C5)**.

Foltz, G. R., C. Schmid, and R. Lumpkin, 2018: An enhanced pirata dataset for tropical atlantic ocean–atmosphere research. *Journal of Climate*, **31 (4)**, 1499–1524.

Gaspar, P., Y. Grégoris, and J.-M. Lefevre, 1990: A simple eddy kinetic energy model for simulations of the oceanic vertical mixing: Tests at station papa and long-term upper ocean study site. *Journal of Geophysical Research: Oceans*, **95 (C9)**, 16 179–16 193.

Goubanova, K., E. Sanchez-Gomez, C. Frauen, and A. Voldoire, 2019: Respective roles of remote and local wind stress forcings in the development of warm sst errors in the south-eastern tropical atlantic in a coupled high-resolution model. *Climate Dynamics*, **52 (3)**, 1359–1382, doi:10.1007/s00382-018-4197-0, URL https://doi.org/10.1007/s00382-018-4197-0.

Harlass, J., M. Latif, and W. Park, 2015: Improving climate model simulation of tropical atlantic sea surface temperature: The importance of enhanced vertical atmosphere model resolution. *Geophysical Research Letters*, **42 (7)**, 2401–2408.

Hartung, K., G. Svensson, H. Struthers, A.-L. Deppenmeier, and W. Hazeleger, 2018: An ec-earth coupled atmosphere–ocean single-column model (aoscm. v1_ec-earth3) for studying coupled marine and polar processes. *Geoscientific Model Development*, **11 (10)**, 4117–4137.

Accepted for publication in *Journal of Climate*. DOI 10.1175/JCLI-D-19-0608.1.

Hazeleger, W., and R. J. Haarsma, 2005: Sensitivity of tropical atlantic climate to mixing in a coupled ocean–atmosphere model. *Climate dynamics*, **25 (4)**, 387–399.

Hazeleger, W., and Coauthors, 2010: Ec-earth: A seamless earth-system prediction approach in action. *Bulletin of the American Meteorological Society*, **91 (10)**.

Hazeleger, W., and Coauthors, 2012: Ec-earth v2. 2: description and validation of a new seamless earth system prediction model. *Climate Dynamics*, **39 (11)**, 2611–2629.

Hourdin, F., A. Găinusă-Bogdan, P. Braconnot, J.-L. Dufresne, A.-K. Traore, and C. Rio, 2015: Air moisture control on ocean surface temperature, hidden key to the warm bias enigma. *Geophysical Research Letters*, **42 (24)**, 10–885.

Hu, Z.-Z., B. Huang, Y.-T. Hou, W. Wang, F. Yang, C. Stan, and E. K. Schneider, 2011: Sensitivity of tropical climate to low-level clouds in the ncep climate forecast system. *Climate dynamics*, **36 (9-10)**, 1795–1811.

Hu, Z.-Z., B. Huang, and K. Pegion, 2008: Low cloud errors over the southeastern atlantic in the ncep cfs and their association with lower-tropospheric stability and air-sea interaction. *Journal of Geophysical Research: Atmospheres*, **113 (D12)**.

Huang, B., Z.-Z. Hu, and B. Jha, 2007: Evolution of model systematic errors in the tropical atlantic basin from coupled climate hindcasts. *Climate dynamics*, **28 (7-8)**, 661–682.

Hummels, R., M. Dengler, P. Brandt, and M. Schlundt, 2014: Diapycnal heat flux and mixed layer heat budget within the atlantic cold tongue. *Climate dynamics*, **43 (11)**, 3179–3199.

Koseki, S., N. Keenlyside, T. Demissie, T. Toniazzo, F. Counillon, I. Bethke, M. Ilicak, and M.-L. Shen, 2018: Causes of the large warm bias in the angola–benguela frontal zone in the norwegian earth system model. *Climate Dynamics*, **50 (11-12)**, 4651–4670.

Accepted for publication in *Journal of Climate*. DOI 10.1175/JCLI-D-19-0608.1.

Lilly, D., D. Waco, and S. Adelfang, 1974: Stratospheric mixing estimated from high-altitude turbulence measurements. *Journal of Applied Meteorology*, **13 (4)**, 488–493.

Ma, C.-C., C. R. Mechoso, A. W. Robertson, and A. Arakawa, 1996: Peruvian stratus clouds and the tropical pacific circulation: A coupled ocean-atmosphere gcm study. *Journal of Climate*, **9 (7)**, 1635–1645.

Madec, G., and Coauthors, 2011: Nemo ocean engine.

Milinski, S., J. Bader, H. Haak, A. C. Siongco, and J. H. Jungclaus, 2016: High atmospheric horizontal resolution eliminates the wind-driven coastal warm bias in the southeastern tropical atlantic. *Geophysical Research Letters*, **43 (19)**, 10–455.

Moum, J. N., D. R. Caldwell, and C. A. Paulson, 1989: Mixing in the equatorial surface layer and thermocline. *Journal of Geophysical Research: Oceans*, **94 (C2)**, 2005–2022.

Moum, J. N., A. Perlin, J. D. Nash, and M. J. McPhaden, 2013: Seasonal sea surface cooling in the equatorial pacific cold tongue controlled by ocean mixing. *Nature*, **500 (7460)**, 64.

Oakey, N., 1982: Determination of the rate of dissipation of turbulent energy from simultaneous temperature and velocity shear microstructure measurements. *Journal of Physical Oceanography*, **12 (3)**, 256–271.

Osborn, T., 1980: Estimates of the local rate of vertical diffusion from dissipation measurements. *Journal of Physical Oceanography*, **10 (1)**, 83–89.

Planton, Y., A. Voldoire, H. Giordani, and G. Caniaux, 2018: Main processes of the atlantic cold tongue interannual variability. *Climate Dynamics*, **50 (5-6)**, 1495–1512.

Richter, I., and S.-P. Xie, 2008: On the origin of equatorial atlantic biases in coupled general circulation models. *Climate Dynamics*, **31 (5)**, 587–598.

Accepted for publication in *Journal of Climate*. DOI 10.1175/JCLI-D-19-0608.1.

Richter, I., S.-P. Xie, A. T. Wittenberg, and Y. Masumoto, 2012: Tropical atlantic biases and their relation to surface wind stress and terrestrial precipitation. *Climate dynamics*, **38 (5-6)**, 985–1001.

Rouault, M., J. Servain, C. Reason, B. Bourlès, M. Rouault, and N. Fauchereau, 2009: Extension of pirata in the tropical south-east atlantic: an initial one-year experiment. *African Journal of Marine Science*, **31 (1)**, 63–71, doi:10.2989/AJMS.2009.31.1.5.776.

Scannell, H. A., and M. J. McPhaden, 2018: Seasonal mixed layer temperature balance in the southeastern tropical atlantic. *Journal of Geophysical Research: Oceans*, **123 (8)**, 5557–5570.

Seo, H., M. Jochum, R. Murtugudde, and A. J. Miller, 2006: Effect of ocean mesoscale variability on the mean state of tropical atlantic climate. *Geophysical research letters*, **33 (9)**.

Servain, J., A. Busalacchi, M. J. McPhaden, A. D. Moura, and Coauthors, 1998: A pilot research moored array in the tropical atlantic (pirata). *Bulletin of the American Meteorological Society*, **79 (10)**, 2019.

Skyllingstad, E. D., and D. W. Denbo, 1995: An ocean large-eddy simulation of langmuir circulations and convection in the surface mixed layer. *Journal of Geophysical Research: Oceans*, **100 (C5)**, 8501–8522.

Small, R. J., and Coauthors, 2014: A new synoptic scale resolving global climate simulation using the community earth system model. *Journal of Advances in Modeling Earth Systems*, **6 (4)**, 1065–1094.

Stockdale, T. N., M. A. Balmaseda, and A. Vidard, 2006: Tropical atlantic sst prediction with coupled ocean–atmosphere gcms. *Journal of climate*, **19 (23)**, 6047–6061.

Talley, L. D., 2011: *Descriptive physical oceanography: an introduction*. Academic press.

Accepted for publication in *Journal of Climate*. DOI 10.1175/JCLI-D-19-0608.1.

Toniazzo, T., and S. Woolnough, 2014: Development of warm sst errors in the southern tropical atlantic in cmip5 decadal hindcasts. *Climate Dynamics*, **43 (11)**, 2889–2913, doi: 10.1007/s00382-013-1691-2, URL https://doi.org/10.1007/s00382-013-1691-2.

Valcke, S., 2013: The oasis3 coupler: a european climate modelling community software. *Geoscientific Model Development*, **6 (2)**, 373–388.

Vancoppenolle, M., T. Fichefet, H. Goosse, S. Bouillon, C. K. Beatty, and M. Morales Maqueda, 2008: Lim3, an advanced sea-ice model for climate simulation and operational oceanography. *Mercator Ocean Q Newslett*, **28**, 16–21.

Voldoire, A., M. Claudon, G. Caniaux, H. Giordani, and R. Roehrig, 2014: Are atmospheric biases responsible for the tropical atlantic sst biases in the cnrm-cm5 coupled model? *Climate dynamics*, **43 (11)**, 2963–2984.

Voldoire, A., and Coauthors, 2019: Role of wind stress in driving sst biases in the tropical atlantic. *Climate Dynamics*, 1–24.

Wang, C., L. Zhang, S.-K. Lee, L. Wu, and C. R. Mechoso, 2014: A global perspective on cmip5 climate model biases. *Nature Climate Change*, **4 (3)**, 201.

Weinstock, J., 1978: Vertical turbulent diffusion in a stably stratified fluid. *Journal of the Atmospheric Sciences*, **35 (6)**, 1022–1027.

Xu, Z., P. Chang, I. Richter, and G. Tang, 2014a: Diagnosing southeast tropical atlantic sst and ocean circulation biases in the cmip5 ensemble. *Climate dynamics*, **43 (11)**, 3123–3145.

Xu, Z., M. Li, C. M. Patricola, and P. Chang, 2014b: Oceanic origin of southeast tropical atlantic biases. *Climate dynamics*, **43 (11)**, 2915–2930.

Accepted for publication in *Journal of Climate*. DOI 10.1175/JCLI-D-19-0608.1.

Zuidema, P., and Coauthors, 2016: Challenges and prospects for reducing coupled climate model sst biases in the eastern tropical atlantic and pacific oceans: The us clivar eastern tropical oceans synthesis working group. *Bulletin of the American Meteorological Society*, **97 (12)**, 2305–2328.

Accepted for publication in *Journal of Climate*. DOI 10.1175/JCLI-D-19-0608.1.

LIST OF TABLES

Accepted for publication in *Journal of Climate*. DOI 10.1175/JCLI-D-19-0608.1.

Experiment	Description	RMSE SST	RMSE SSR
Control	Coupled SCM, atmosphere driven by T,Q,U, and V advection from ERA-Interim, and relaxed above 3 km with τ_a = 6 hours.	1.25 ^{o}C	103 W/m^2
Shortwave	Coupled SCM, ocean forced with shortwave radiation from PIRATA buoy observation.	1.33 ^{o}C	0 W/m^2
Atm ERA	Horizontal wind components U,V and T and Q profiles from ERA-Interim nudged down to the surface.	0.70 ^{o}C	94 W/m^2
U,V ERA	Horizontal wind components U,V from ERA-Interim nudged down to the surface, T and Q atmospheric profiles from control simulation.	1.28^{o}C	101 W/m^2
T,Q ERA	T and Q profiles from ERA-Interim nudged down to the surface, U and V from control simulation.	0.69 ^{o}C	95 W/m^2
C_{LC} sweep	Coupled SCM in different configurations as described above, with varying Langmuir coefficient.	0.83 ^{o}C *	96 W/m^2 *
C_{diff} sweep	As C_{LC} sweep, but with varying coefficient $C_{diff}$for turbulent coefficient A_{vt} calculation.	0.34 ^{o}C *	102 W/m^2 *
$N^2{}_{PIR}$	Coupled SCM, but turbulent coefficients are calculated from PIRATA temperature and salinity profiles from buoy data.	0.89 ^{o}C	97 W/m^2

TABLE 1. Sensitivity experiments performed with the coupled SCM, and their overall root mean square SST and surface shortwave radiation (SSR) biases with respect to PIRATA observation. The upper part of the table lists experiments with changes in the atmosphere, while the lower part of the table lists experiments with changes in the ocean. All experiments are performed for the period of June 1st – 30th in 2014. * For the sweeps we note the minimum RMSE at optimal parameter value.

Accepted for publication in *Journal of Climate*. DOI10.1175/JCLI-D-19-0608.1.

LIST OF FIGURES

Accepted for publication in *Journal of Climate*. DOI10.1175/JCLI-D-19-0608.1.

Accepted for publication in *Journal of Climate*. DOI 10.1175/JCLI-D-19-0608.1.

FIG. 1. Seasonal cycle of surface temperatures in the tropical Atlantic from ERA-Interim reanalysis data (Dee et al. 2011) (1979-2013) (panel a). The star marks the location of the buoy we use in this study, at 8^{o}E, 6^{o}S. It is part of the PIRATA array (Servain et al. 1998; Bourlès et al. 2008). Panel b shows the seasonal cycle of SST from buoy data, averaged from daily data over the years 2014-2018, and for the coupled global version of EC-Earth.

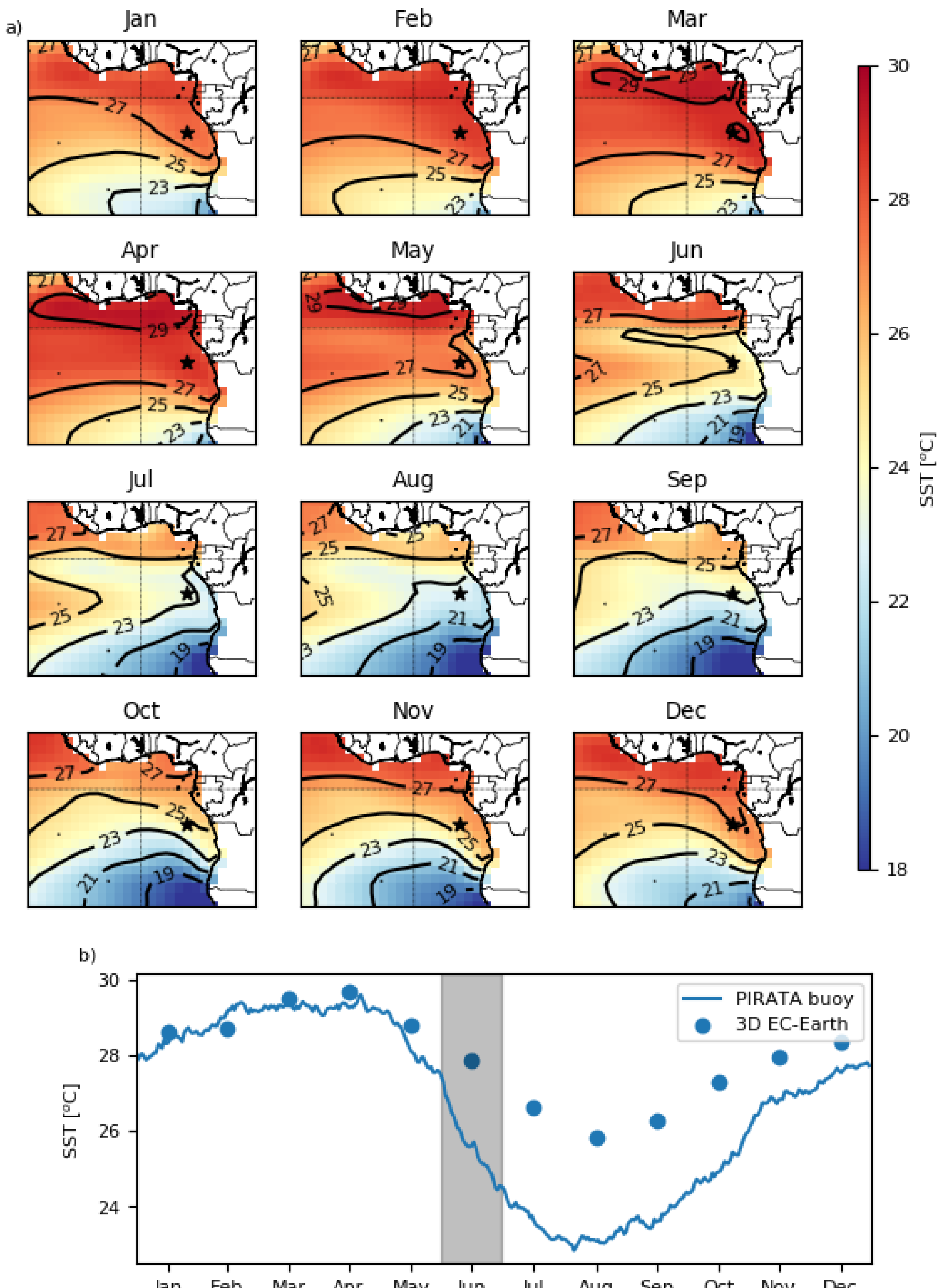

Accepted for publication in *Journal of Climate*. DOI 10.1175/JCLI-D-19-0608.1.

FIG. 2. Schematic of the coupled ocean atmosphere SCM version of EC-Earth used in this study. We force the atmosphere with temperature, moisture, and momentum advection. At the interface between the atmosphere and the ocean the model components exchange fluxes, among which the turbulent (latent and sensible heatflux, LH+SH) and radiative heat fluxes (shortwave (SW) and longwave (LW)) indicated with arrows. The ocean further receives momentum forcing from the atmosphere (τ), and mass fluxes (not indicated). In the ocean column, vertical mixing is the only parameterized process solved for with the TKE scheme (Mix_{TKE}).

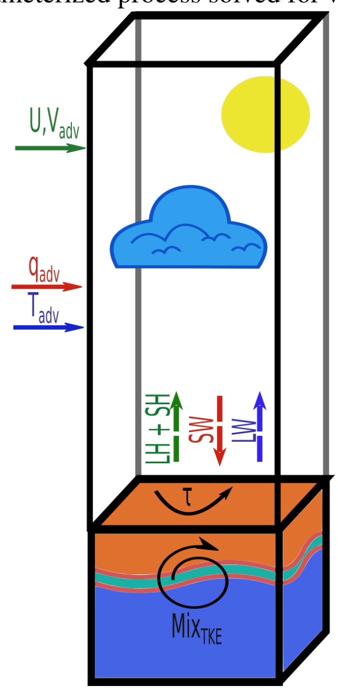

Accepted for publication in *Journal of Climate*. DOI 10.1175/JCLI-D-19-0608.1.

FIG. 3. Average SST at the buoy location at 6^{o}South, 8^{o}East in June for the years 2014-2018.

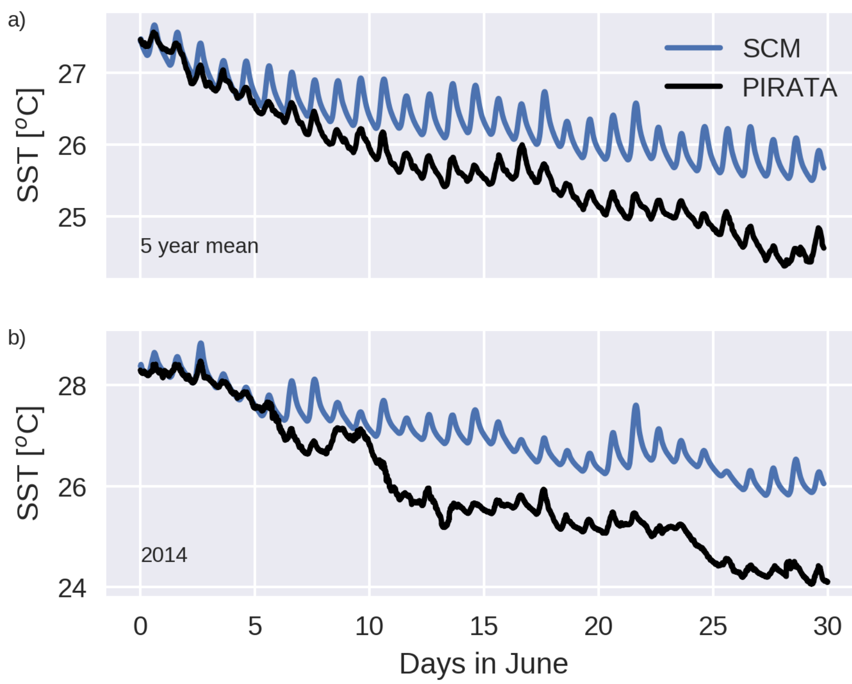

Accepted for publication in *Journal of Climate*. DOI 10.1175/JCLI-D-19-0608.1.

FIG. 4. June 2014 atmosphere specific humidity (top row), atmospheric temperature (centre row) and ocean temperature (bottom row) at the buoy location at 6^{o}South, 8^{o}East in June, atmospheric data from ERA-Interim and ocean temperature from PIRATA data, and as modelled by the SCM (control). Ticks on the right hand sides of the bottom row indicate levels at which ocean data is available. Atmospheric data is available on the same model level heights for ERA-Interim and the SCM.

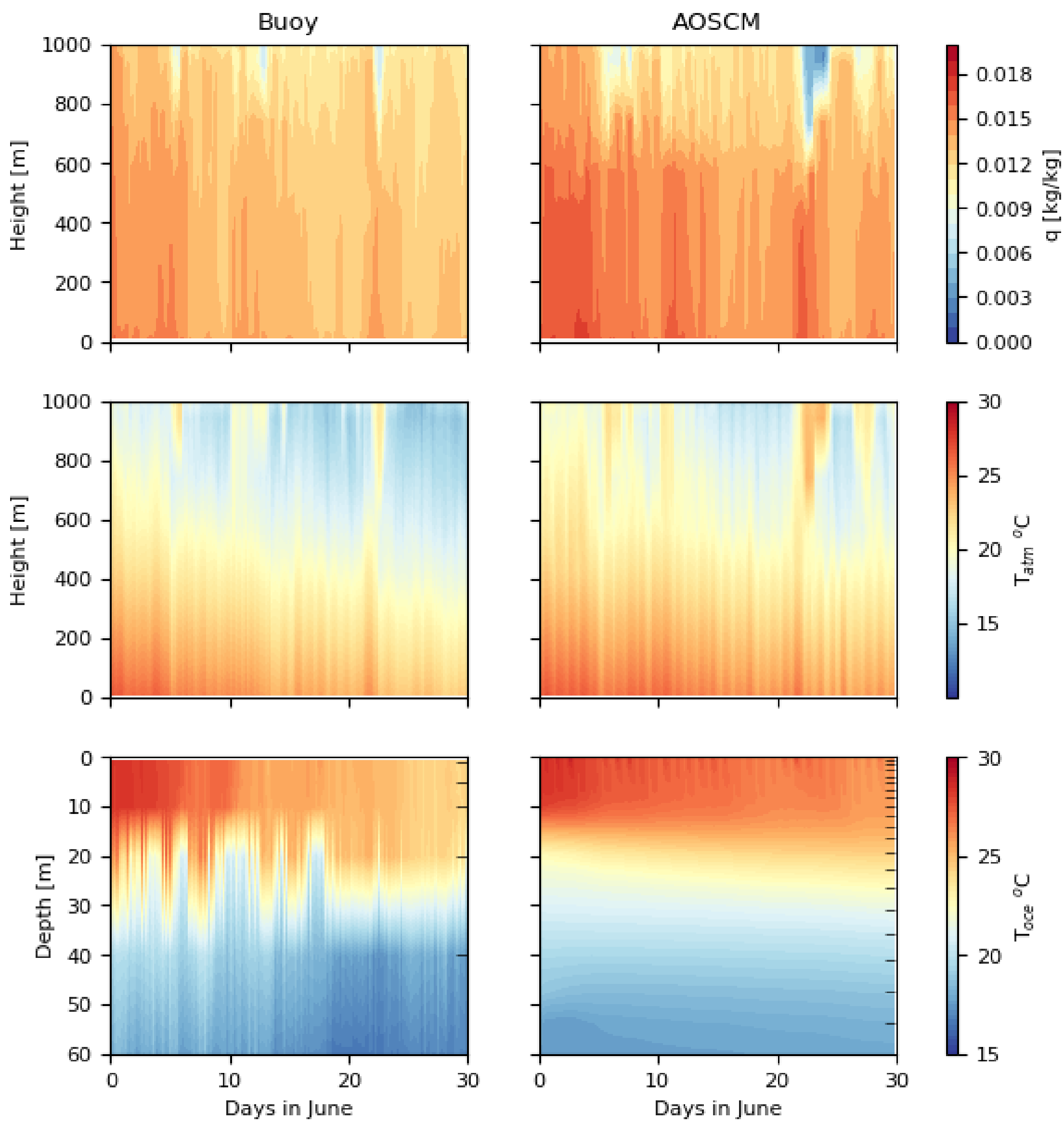

Accepted for publication in *Journal of Climate*. DOI 10.1175/JCLI-D-19-0608.1.

765 FIG. 5. Control simulation (June 2014) surface fluxes, net shortwave (red, SW), net longwave (blue, LW),
766 and the turbulent fluxes latent heat and sensible heat combined (green, LH + SH). Of the latter, latent heat is the
767 much larger contribution. The sum of the surface fluxes is shown in black (TOT).

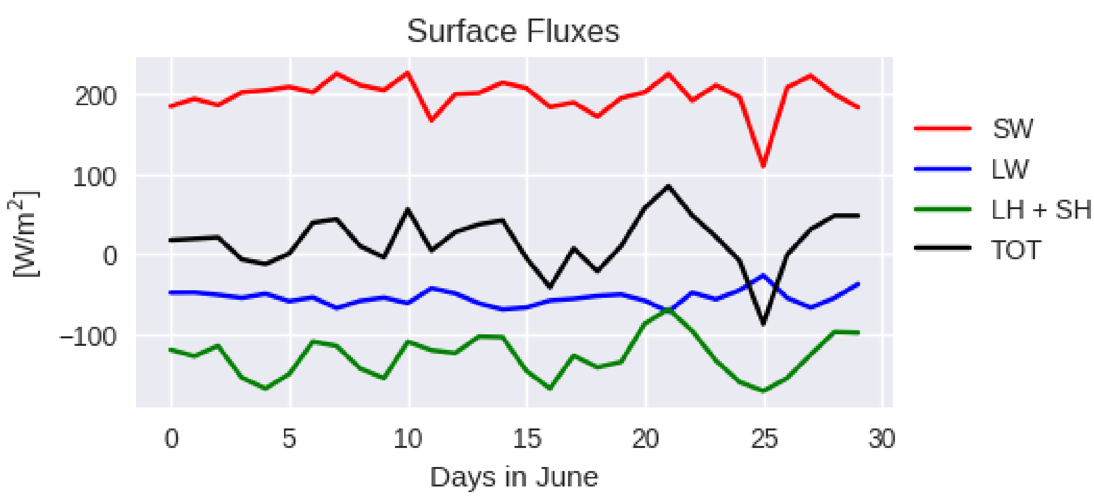

Accepted for publication in *Journal of Climate*. DOI 10.1175/JCLI-D-19-0608.1.

768 FIG. 6. Downward shortwave radiation from the PIRATA buoy and from the SCM control run, at 2 minute
769 and 15 minute temporal resolution, respectively.

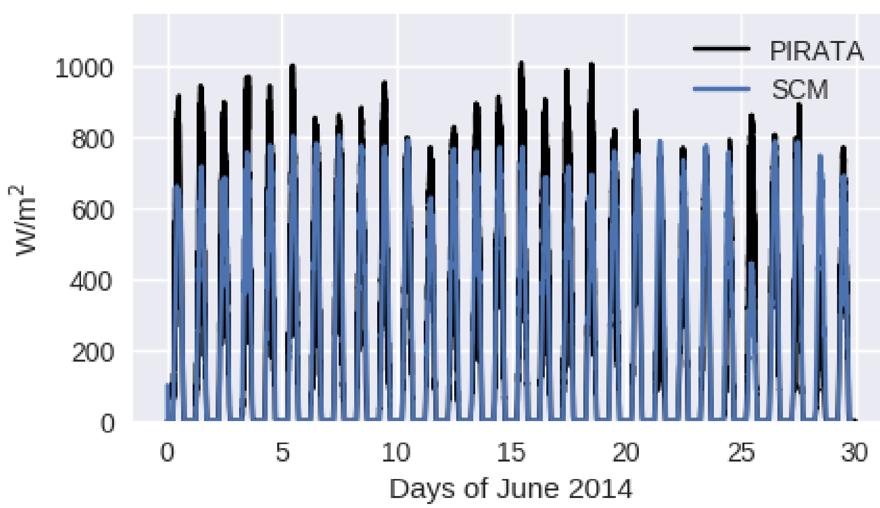

Accepted for publication in *Journal of Climate*. DOI 10.1175/JCLI-D-19-0608.1.

FIG. 7. Daily integrals of the downwards shortwave radiation flux during June from the PIRATA buoy, from data received at 2 minute intervals, and interpolated to model timestep resolution of 15 minutes, and from the SCM control run.

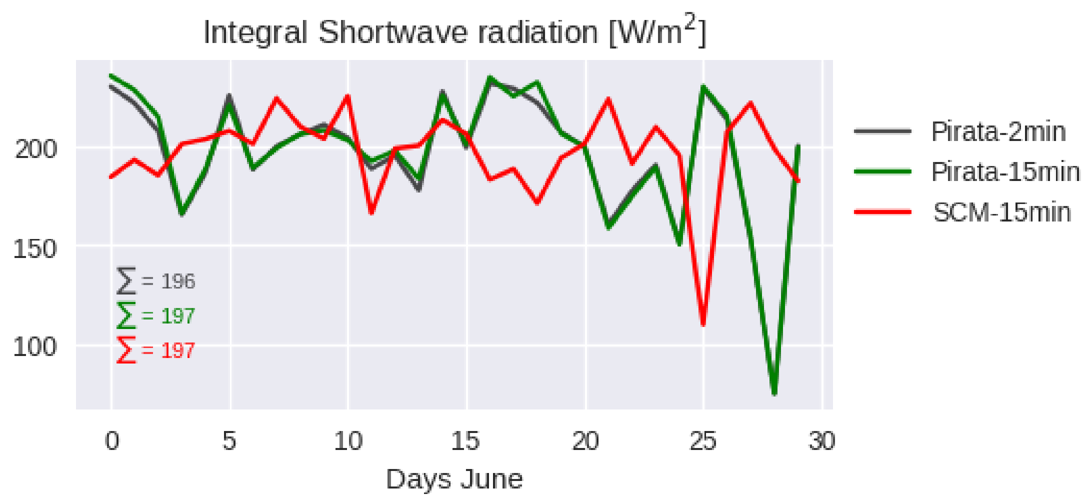

Accepted for publication in *Journal of Climate*. DOI 10.1175/JCLI-D-19-0608.1.

FIG. 8. SST as simulated by the various atmospheric experiments described in the upper part of Table 1. The black line shows observed SST for comparison.

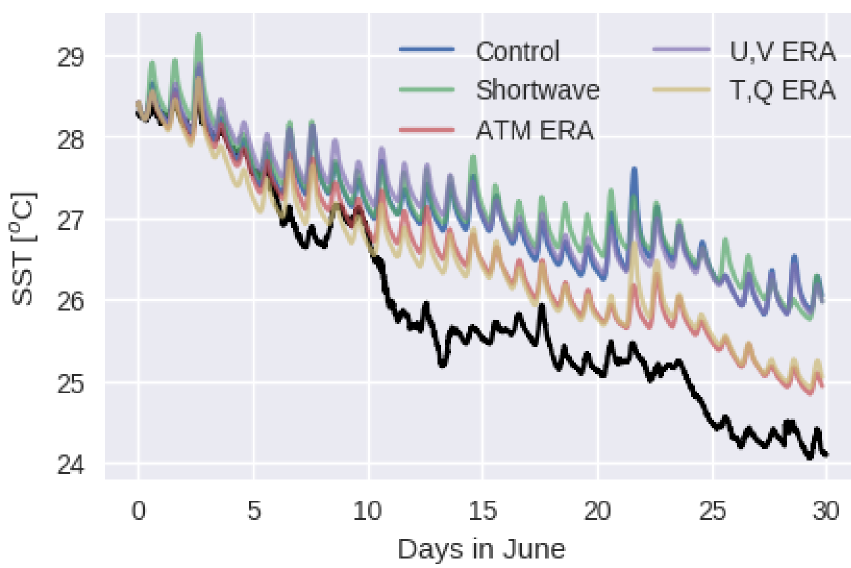

Accepted for publication in *Journal of Climate*. DOI 10.1175/JCLI-D-19-0608.1.

FIG. 9. Panel a) shows surface fluxes as in Fig. 5, net surface shortwave radiation in red, net surface longwave in blue, turbulent fluxes in green, and total sum of fluxes in black. The control experiments is depicted in solid faded lines, Atm ERA in dashed lines, T,Q ERA in dotted lines, and U,V ERA in dashed-dotted lines. Panel b) shows the relative change of integrated surface fluxes with respect to the control experiment, in percent. Colours as in panel a). Note that due to the sign convention an increase in turbulent as well as longwave radiative flux translates to an increased in cooling.

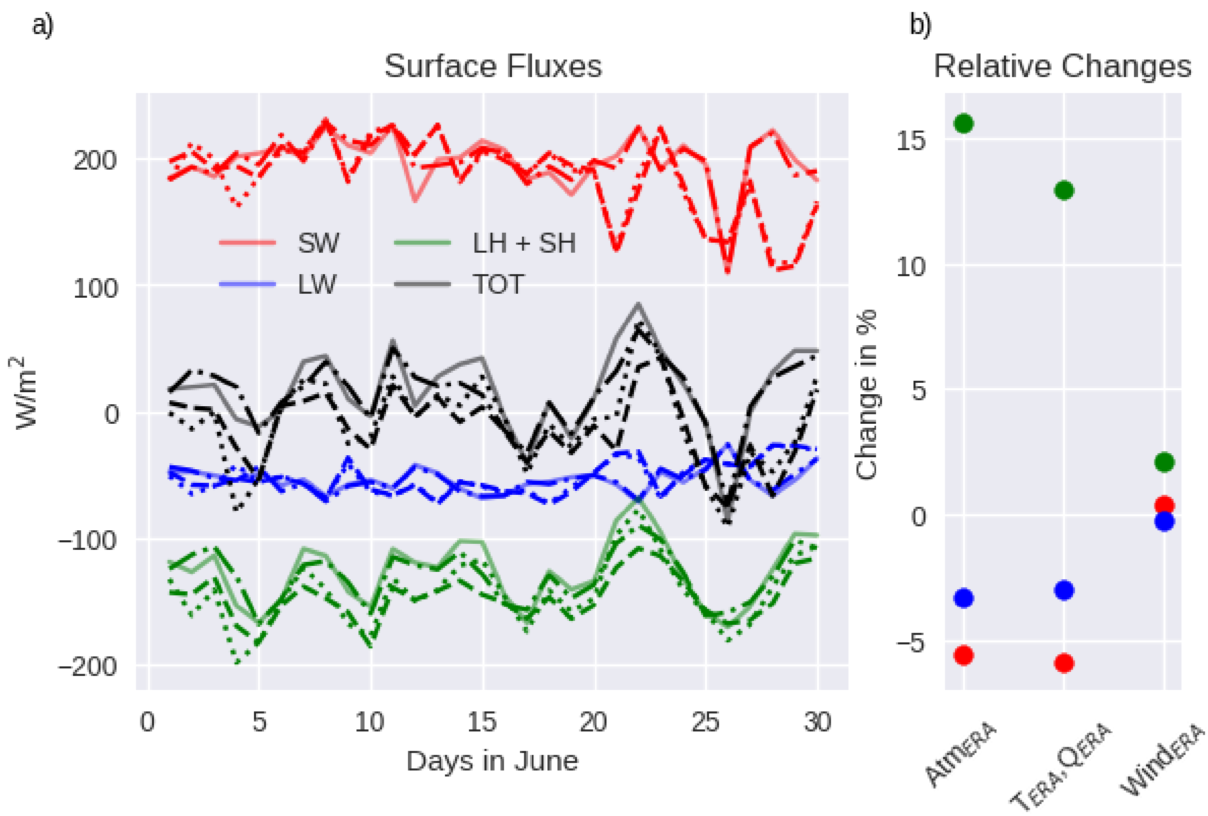

Accepted for publication in *Journal of Climate*. DOI 10.1175/JCLI-D-19-0608.1.

FIG. 10. Root mean square SST errors in the parameter sweeps for C_{LC} and C_{diff}.

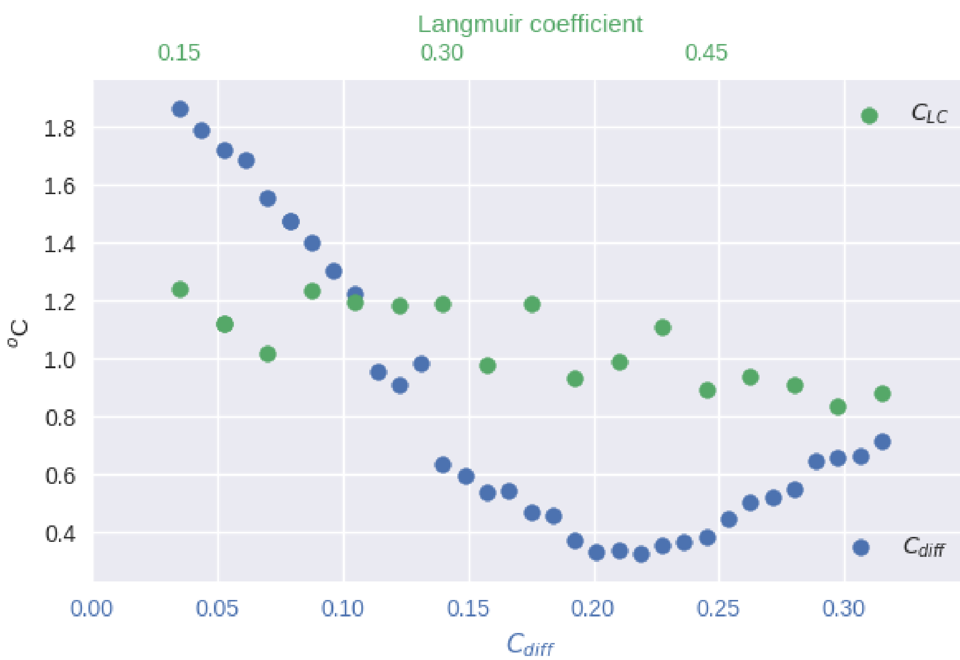

Accepted for publication in *Journal of Climate*. DOI 10.1175/JCLI-D-19-0608.1.

781 FIG. 11. SST as simulated by the various oceanic experiments described in the lower part of Table 1. The

782 black line shows observed SST for comparison.

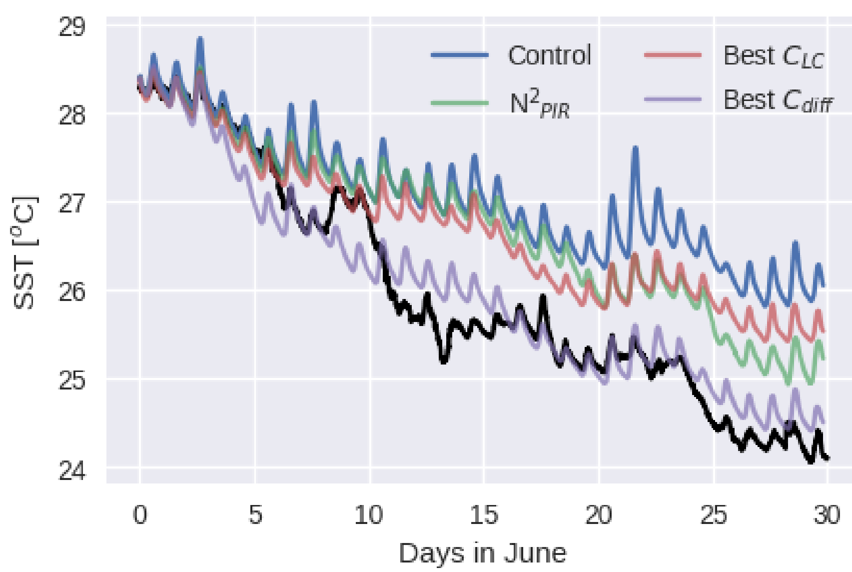

Accepted for publication in *Journal of Climate*. DOI 10.1175/JCLI-D-19-0608.1.

FIG. 12. Atmospheric moisture (upper row), temperature (centre row), and upper ocean temperature (bottom row) in the control experiment and at ideal C_{diff}.

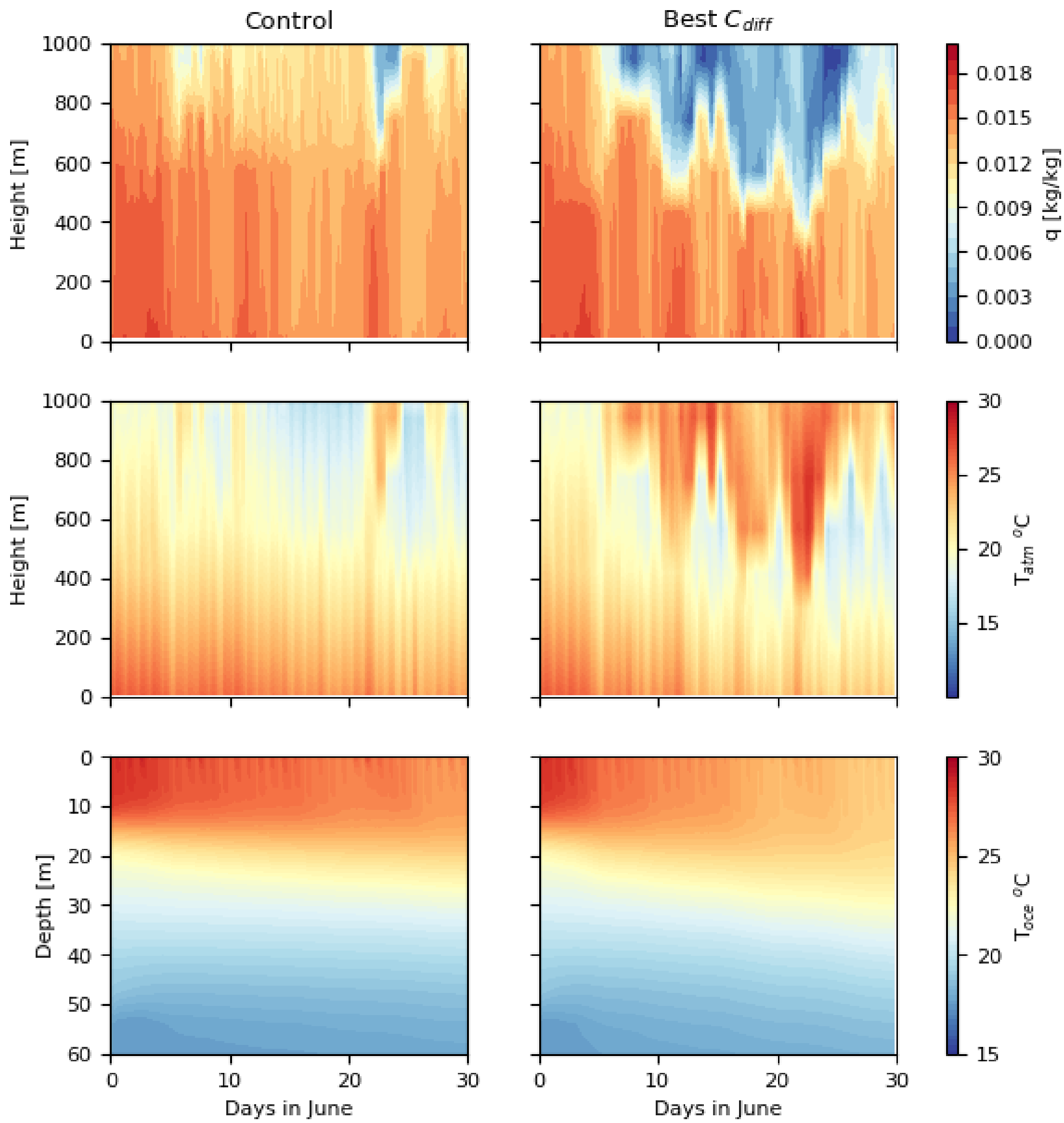

Accepted for publication in *Journal of Climate*. DOI 10.1175/JCLI-D-19-0608.1.

FIG. 13. Integrated surface fluxes over the time of the simulations in the C_{diff} sweep. Turbulent components latent and sensible heat fluxes are combined in green, the radiative components shortwave and longwave are in red and blue, respectively.

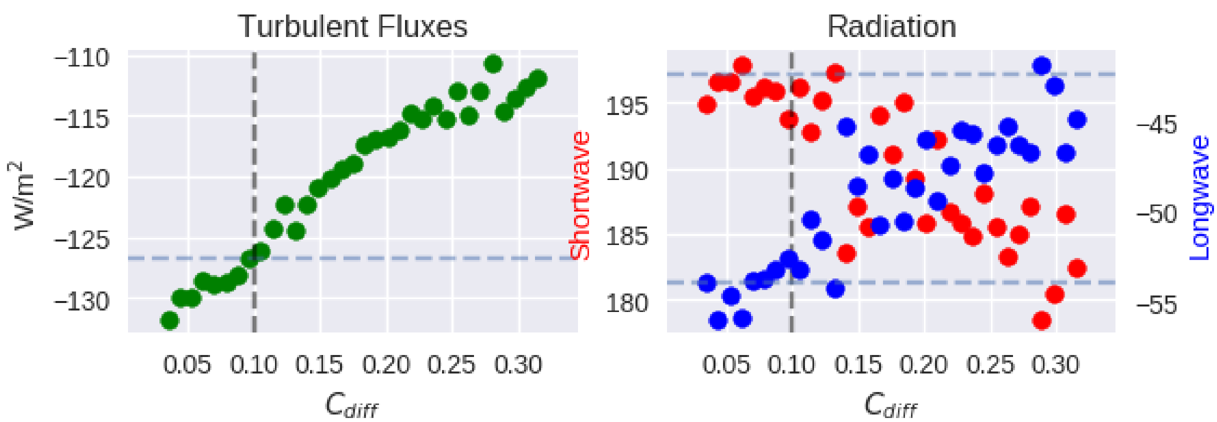

Accepted for publication in *Journal of Climate*. DOI 10.1175/JCLI-D-19-0608.1.

FIG. 14. Root mean square SST errors in the parameter sweeps for C_{diff}, with cubic fits. Stars mark the minimum SST RMSE on the fit.

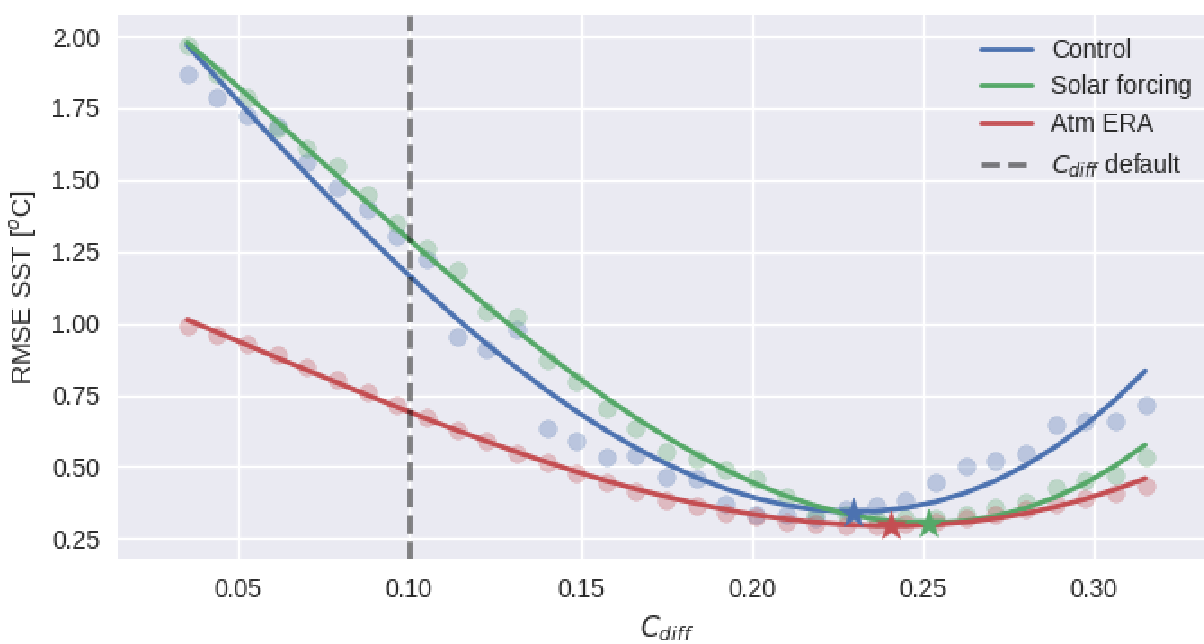

Accepted for publication in *Journal of Climate*. DOI 10.1175/JCLI-D-19-0608.1.